Marine and Petroleum Geology 135 (2022) 105404

Contents lists available at ScienceDirect

Marine and Petroleum Geology

journal homepage: www.elsevier.com/locate/marpetgeo

Organic matter enrichment of the Chang 7 member in the Ordos Basin: Insights from chemometrics and element geochemistry

Jun Shi [a,c], Yan-Rong Zou [a,b], Yu-Lan Cai [a,b], Zhao-Wen Zhan [a,b,*], Jia-Nan Sun [a,c], Tian Liang [a,c], Ping'an Peng [a,b]

[a] State Key Laboratory of Organic Geochemistry, Guangzhou Institute of Geochemistry, Chinese Academy of Sciences, Guangzhou, 510640, China
[b] CAS Center for Excellence in Deep Earth Science, Guangzhou, 510640, China
[c] University of Chinese Academy of Sciences, Beijing, 100049, China

ARTICLE INFO

Keywords:
Organic matter enrichment
Palaeoenvironment
Chemometrics
Element geochemistry
Principal component analysis

ABSTRACT

The lacustrine black shales of the Chang 7 member are the main source rocks and the most important unconventional (shale oil) petroleum resources in the Ordos Basin, North China. A series of continuous core samples was analysed for main, trace, and rare earth elements. The development of thin or laminar tuffs and tuffaceous mudstones and the enrichment of Fe, Mn, and other elements demonstrate that the Chang 7 member was influenced by event deposition, such as volcanic and hydrothermal activity. The ancient lake had brackish water and a relatively high sedimentation rate during the deposition of the Chang 7 member. The palaeoclimate in the early stage was warmer and wetter than that in the middle-late stage of the Chang 7 period. The geochemical proxies for palaeoproductivity and palaeoredox indicate that the ancient lake had a relatively high primary productivity with an anoxic to euxinic sulphide bottom water in the Chang 7^3 stage, which decreased to dyoxic-oxic water during the Chang 7^{1+2} periods. A parameter dataset comprising 11 elemental proxies related to the reconstruction or evaluation of the depositional environment and palaeoproductivity was analysed using principal component analysis (PCA). The first principal component (PC1) accounted for 59.88% of the total variance in the original dataset and mainly represented the characteristics of palaeoproductivity and redox conditions; thus, it can be interpreted as an indicator of these factors. Based on the excellent positive linear correlation between the total organic matter content of the Chang 7 samples and the PC1 scores, the enrichment of organic matter in the Chang 7 member was mainly controlled by palaeoproductivity and the preservation environment. PCA is an effective method for dimensionality reduction and visualisation of multi-element geochemical data, which allows for a more comprehensive and in-depth understanding of geological samples. This work provides a practical application of chemometrics in elemental geochemistry. This can serve as a model for other studies.

1. Introduction

The preservation of organic matter involves many physicochemical processes and factors, including nutrient availability, volcanism and hydrothermal activities, primary productivity, redox conditions, sedimentation rate, and post-depositional degradation processes (Murphy et al., 2000; Lash and Blood, 2014). These have been summarised into three simple models—productivity, preservation and sedimentation rate—to explain the enrichment of organic matter (Tyson, 2005; Katz, 2005). The productivity model emphasises that high primary productivity leads to a large accumulation of organic matter, which is induced by a high nutrient supply from sedimentary environments (Pedersen and Calvert, 1990; Parrish, 1995). The preservation model assumes that a dyoxic/anoxic sedimentary bottom water environment is the main control of organic matter preservation, which improves organic matter accumulation by reducing its consumption and limiting the benthic activity in the processes of organic matter deposition and post-deposition (Demaison and Moore, 1980). The sedimentation rate model suggests that there is a critical threshold for the sedimentation rate: the amount of accumulated organic matter increases with the sedimentation rate until the threshold is reached; once it is exceeded and the sedimentation rate continues to increase, the amount of organic

* Corresponding author. State Key Laboratory of Organic Geochemistry, Guangzhou Institute of Geochemistry, Chinese Academy of Sciences, Guangzhou, 510640, China.
E-mail address: zhanzw@gig.ac.cn (Z.-W. Zhan).

https://doi.org/10.1016/j.marpetgeo.2021.105404
Received 6 January 2021; Received in revised form 21 August 2021; Accepted 26 October 2021
Available online 28 October 2021

matter decreases due to dilution (Ibach, 1982; Murphy et al., 2000). However, in many cases, no single factor or mode can dominate and explain the complex process, which is often controlled by multiple factors.

Various geochemical data, including petrological and mineralogical data, organic and inorganic data, and molecular and isotopic data, have been proposed to characterise the factors controlling the enrichment of organic matter in black shale. For example, palaeoproductivity may be affected by palaeoclimate, biological primary productivity, and event deposition (volcanic and hydrothermal activity, etc.) (Chen et al., 2020). Palaeoclimate conditions can be evaluated by the distribution or ratio of major and trace elements (e.g., Ga/Rb vs K_2O/Al_2O_3, chemical index of alteration, palaeoclimate index, Sr/Cu, etc.) (McLennan, 1993; Roy and Roser, 2013; Li et al., 2020). Primary productivity can be reconstructed by taking advantage of a variety of geochemical proxies, such as organic carbon (C_{org}), carbon and nitrogen isotopes ($\delta^{13}C_{car}$, $\delta^{13}C_{om}$, and $\delta^{15}N$), organic biomarkers, and essential nutrients and life structural elements (Cu, Zn, Ba, P, etc.) (Algeo and Maynard, 2004; Tribovillard et al., 2006). Event deposition can be detected by some phenomena and indicators, such as the development of tuff and tuffaceous mudstone, mineral assemblages of hematite–pyrite–anhydrite, and platinum group elements (PGEs). (Bau et al., 2014; Qiu et al., 2015; Liao et al., 2019; Zhang et al., 2020). Palaeoredox can be reconstructed using a series of geochemical parameters, such as biomarker molecular ratios (pristine/phytane, homohopane index, etc.), abundances and relationships of redox-sensitive trace elements (Mo–U covariation, Fe speciation, C_{org}:P molar ratio, U/Th, etc.), and anomalies of rare earth elements (REEs) (Ce, Eu) (Peters et al., 2005; Algeo and Tribovillard, 2009; Tribovillard et al., 2012). Palaeosalinity can be distinguished by a series of indices, such as the abundance and ratios of organic matter and S, Sr and Ba, Rb and K, and B and Ga (Wei and Algeo, 2020). The deposition rate can be measured by the abundance and differentiation characteristics of REEs (Johannesson et al., 1994; Chen et al., 2019). Although there are many proxies that can be used to identify the main controlling factors of organic matter enrichment, no single proxy can be used independently to characterise a factor under all conditions. All indicators have an optimal application range and great uncertainty, which makes it feasible to use multiple indicators for comprehensive analysis or mutual support. The comprehensive application of multiple parameters is beneficial for a deeper understanding of geological samples.

Chemometrics uses multivariate statistics to recognise patterns and extract comprehensive and useful information from all types of measurement data. Compared with the traditional univariate or bivariate analysis techniques, which only deal with one or two variables (proxies) at a time, multivariate techniques treat all data (proxies) simultaneously using matrix algebra and describe a sample by a point in space that has as many axes as variables (Peters et al., 2005). This allows for a more comprehensive and in-depth understanding of geological samples. In this study, chemometrics was used to process a dataset consisting of a series of geochemical proxies of different types and meanings to understand the enrichment mechanism and main controlling factors of organic matter in lacustrine source rocks of the Chang 7 member of the Yanchang Formation in the southeastern Ordos Basin, North China. The aim is to better understand the genesis of high-quality source rocks in the study area, and to provide a practical application of chemometrics in elemental geochemistry.

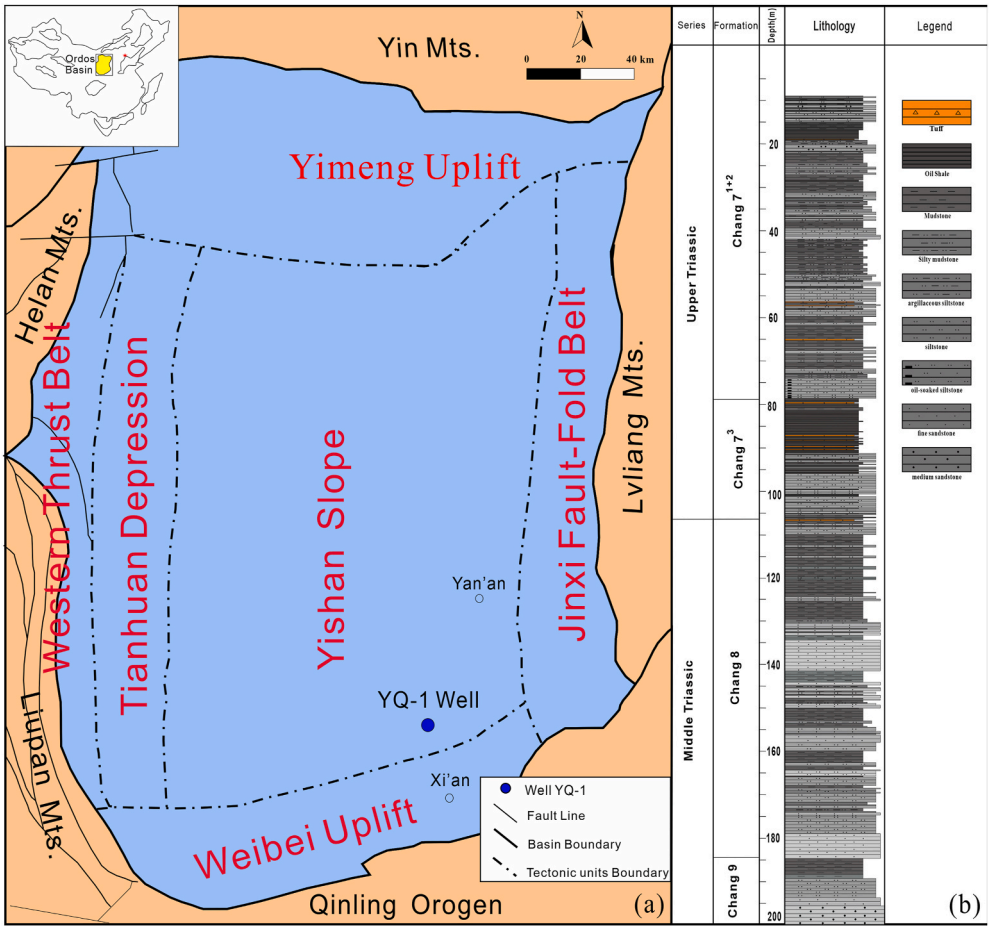

Fig. 1. Map showing (a) the location and tectonic units of the Ordos Basin, and (b) the stratigraphy and lithology in the study area region of the Yanchang Formation.

2. Geological setting

The Ordos Basin, located in central northern China, is one of the most important terrestrial petroliferous basins in China. In a tectonic sense, the Ordos Basin is a part of the North China Block and bordered to the north, east, south, and west by the Yin, Lvliang, Qinling, Liupan, and Helan Mountains, respectively (Fig. 1). The Ordos Basin is a typical multicylcle cratonic depression basin developed on the base of Archean granulites and the lower Proterozoic greenschists of the North China Block. The evolution of the Ordos Basin mainly comprises four stages: the Early Palaeozoic shallow marine platform, the Late Palaeozoic offshore plain, the Mesozoic intracontinental basin, and Cenozoic faulting and subsidence (Qiu et al., 2014). Six tectonic units, including the Yimeng Uplift, Western Thrust Belt, Tianhuan Depression, Yishan Slope, Weibei Uplift, and Jinxi Fault-Fold Belt, compose the Ordos Basin (Zhang et al., 2020). The study area is located in the Yishan Slope on the southeastern margin of the basin (Fig. 1).

During the late Palaeozoic, the Ordos Basin was in a period of overall uplift, and the southern margin experienced collisional orogenesis. In the Early to Middle Trassic period, the North China Block collided with the Yangtze Block, which led to the formation of the Qinling Mountains (Yang et al., 2005). In the Middle Triassic period, continental clasts increased southward, and the terrestrial facies gradually dominated in the Ordos Basin due to seawater retrogradation from north to south. In the Late Triassic period, the progressive closure of the basin completed the transformation from marine sedimentary facies to terrestrial lake basin. Volcanic and hydrothermal activities were frequent along the southern margin of the basin (Zhang et al., 2020; Ji et al., 2021). Furthermore, the intense regional tectonic activities led to the maximum lake extent during the Late Triassic, which was conducive to the formation of high-quality source rocks, the deposits of the Yanchang Formation of the Upper Triassic. The integrated progradation-aggradation-retrogradation sedimentary sequence of sand and shale sediments in the Yanchang Formation of the Upper Triassic is a record of the complete evolution of the lake basin (Qiu et al., 2015). The Yanchang Formation was divided into 10 members based on rhythmic lithological alterations, including the members Chang 1 to Chang 10 from top to bottom. The Chang 7 member developed in the middle-lower part of the Yanchang Formation with approximately 100–120 m thickness. The lake basin expanded to its maximum in the early Chang 7 member and then gradually shrunk. Therefore, the sediments changed from shale or carbonaceous shale to mudstone and then to sandy mudstone from the early to the late stages of the Chang 7 member. The lacustrine black shales of the Chang 7 member have a high organic matter abundance, excellent organic matter type, and suitable maturity, and are considered to be the main source rocks and the most important unconventional (shale oil) petroleum resources in the Ordos Basin.

3. Samples and method

3.1. Samples

The total thickness of the drilled core of the Yaoqu 1 well (YQ1) located at the southeastern margin of the Ordos Basin is 200 m and includes Chang 7, Chang 8, and Chang 9 strata of the Yanchang Formation (Fig. 1). The Chang 8 and Chang 9 strata are mainly grey thick layers of fine-grained sandstone with intercalations of silty mudstone and mudstone. The Chang 7 strata, which consist of three units (Zhang et al., 2020), reach 106 m and can be divided into upper and lower members, Chang 7^{1+2} and Chang 7^{3}, respectively. The Chang 7^{1+2} strata are mainly grey–black mudstone and silty mudstone, whereas the Chang7^{3} strata are predominantly black shale with intercalations of grey–black mudstone, tuff, and oil immersion (Fig. 1b).

In this study, 53 samples from the Chang 7 member were selected as the target objects, 22 samples from the Chang 7^{1+2} member, dominated by dark mudstones, and 31 samples of the Chang 7^{3} member, which are dominated by black shale (Table 1). The sampling interval was approximately 1 m for the Chang 7^{3} member. We manually avoided nodules, tuffs, and tuffaceous and pyritiferous fills and layers.

3.2. Experiment

All samples were crushed to powder and sieved using a 120-mesh sieve. Each powder sample was weighed accurately and treated with 10% (vol) hydrochloric acid to remove carbonate and dolomite at 85 °C for 4 h in a water bath in a crucible. The remaining hydrochloric acid was removed fully by rinsing the sample with deionised water at least six times. The residue, with inorganic carbon removed, of each sample was dried at 90 °C and analysed using a LECO CS-344 carbon-sulphur analyser to determine the total organic matter (TOC) and total sulphur (TS) contents. A certified reference material (AR4006) was used for quality control. The instrument accuracy was ±0.5%.

The samples for major and trace element and REE analyses were crushed into 200-mesh size without pollution. For major element analysis: the powder samples were mixed with a solvent containing lithium nitrate and then melted at high temperature. The molten samples were poured into a platinum mould to form flat sheets and then analysed using a PANalytical PW2424 X-ray fluorescence (XRF) spectrometer. The relative standard deviation of the abundance of the major elemental oxides was less than 5%. For trace element and REE analysis: the powder samples were combusted in a muffle oven at 750 °C to sufficiently remove all organic matter before dissolution by acids. The acidolysis of the samples after ignition loss was performed using a four-acid mixture of perchloric acid, nitric acid, hydrofluoric acid and hydrochloric acid. The processed samples were analysed by inductively coupled plasma mass spectrometry (ICP-MS, Agilent 7700x) combined with inductively coupled plasma atomic emission spectrometry (ICP-AES, Agilent VISTA). The spectral interferences between elements were corrected. The detailed analytical procedure was similar to that described by Pi et al. (2013). The standard deviation of the elemental concentration was less than 10%.

3.3. Principal component analysis (PCA)

Principal component analysis (PCA) is a chemometrics method that uses the idea of dimensionality reduction in mathematics to transform multiple indices into a few comprehensive indices that reflect the original information as much as possible, and can accurately calculate the correlation coefficients between each variable and the main principal component (PC) to determine the main control variable of the main PC. According to the scores and loadings of PCA, the classification of samples and internal correlation of variables can be determined directly in visual graphics. In this study, PCA from Pirouette software (version 4.5; Infometrix, Inc.) was employed to process a dataset consisting of geochemical proxies. The PCA settings were: Preprocessing = autoscale, maximum factors = 10, validation method = none, rotation = none, and transforms = none.

4. Results

4.1. TOC and TS

The TOC and TS contents of the Chang 7^{1+2} member samples ranged from 0.66% to 3.83% (average = 1.39%) and from 0.07% to 1.72% (average = 0.37%), respectively. The TOC and TS contents of the Chang 7^{3} member were relatively higher with large variations, ranging from 4.90% to 29.50% (average = 15.24%) and from 1.87% to 9.00% (average = 4.93%; Table 1), respectively. These samples have TS/TOC values of 0.08–0.61 (average = 0.31) and fall in the field of marine and brackish facies on the cross-plot of TOC and TS, based on the criterion recommended by Wei and Algeo (2020) (Fig. 2). There are relatively

Table 1
Sample information and partial geochemical parameters.

Sample	Member	Lithology	Depth (m)	TOC (%)	TS (%)	Parameters used for chemometrics (PCA)										
						P1	P2	P3	P4	P5	P6	P7	P8	P9	P10	P11
YQ01	Chang 7^{1+2}	Mudstane	25.91	0.66	0.07	0.02	0.21	0.48	4.31	68.75	0.38	7.72	26.72	−153.42	0.73	8.44
YQ02	Chang 7^{1+2}	Mudstane	27.37	1.08	0.37	0.06	0.22	0.54	3.39	68.93	0.55	10.32	16.12	−20.82	0.61	12.92
YQ03	Chang 7^{1+2}	Mudstane	34.35	1.95	0.65	0.17	0.41	0.46	4.29	63.34	0.44	16.78	27.68	−129.48	0.70	10.03
YQ04	Chang 7^{1+2}	Mudstane	45.09	1.31	0.25	0.06	0.25	0.53	3.97	70.58	0.49	13.78	36.08	−86.88	0.68	10.34
YQ05	Chang 7^{1+2}	Mudstane	49.65	0.99	0.21	0.04	0.25	0.55	3.84	70.91	0.53	10.48	33.08	−36.88	0.66	11.28
YQ06	Chang 7^{1+2}	Mudstane	51.24	1.06	0.36	0.09	0.23	0.53	3.49	70.48	0.40	8.82	21.92	−50.62	0.71	8.01
YQ07	Chang 7^{1+2}	Mudstane	56.67	0.91	0.09	0.03	0.22	0.63	4.15	66.14	0.36	9.12	26.12	−153.82	0.73	8.39
YQ08	Chang 7^{1+2}	Mudstane	57.91	0.68	0.10	0.04	0.21	0.48	4.15	60.49	0.42	7.19	21.44	−202.09	0.76	7.01
YQ09	Chang 7^{1+2}	Mudstane	59.89	0.81	0.17	0.04	0.21	0.38	4.60	69.55	0.65	12.34	23.84	−274.74	0.72	9.40
YQ10	Chang 7^{1+2}	Mudstane	60.89	1.05	0.34	0.10	0.20	0.46	4.10	60.82	0.47	8.73	27.68	−191.23	0.74	7.84
YQ11	Chang 7^{1+2}	Mudstane	62.08	1.06	0.38	0.09	0.25	0.40	4.82	69.46	0.65	20.67	24.52	−229.97	0.71	10.13
YQ12	Chang 7^{1+2}	Mudstane	63.01	0.97	0.20	0.06	0.25	0.54	4.11	53.47	0.37	28.85	44.80	−29.05	0.72	8.15
YQ13	Chang 7^{1+2}	Mudstane	64.70	0.86	0.31	0.07	0.25	0.37	4.10	70.06	0.76	10.58	27.88	−125.18	0.69	10.84
YQ14	Chang 7^{1+2}	Mudstane	65.56	1.00	0.31	0.09	0.23	0.38	4.52	69.22	0.59	13.83	21.28	−200.83	0.74	8.01
YQ15	Chang 7^{1+2}	Mudstane	66.70	3.64	1.72	0.37	0.83	0.31	3.92	66.30	0.73	34.10	28.20	−78.20	0.68	11.51
YQ16	Chang 7^{1+2}	Mudstane	67.51	1.69	0.13	0.05	0.33	0.56	3.90	60.21	0.29	3.82	35.12	−36.82	0.76	6.83
YQ17	Chang 7^{1+2}	Mudstane	68.63	1.10	0.30	0.07	0.23	0.46	3.88	69.94	0.54	15.27	19.92	−140.37	0.70	9.27
YQ18	Chang 7^{1+2}	Mudstane	69.56	1.48	0.25	0.07	0.26	0.49	4.12	54.04	0.43	9.35	22.20	−72.95	0.71	9.22
YQ19	Chang 7^{1+2}	Mudstane	70.65	1.03	0.17	0.08	0.36	0.17	2.58	65.55	0.41	2.86	11.16	−183.76	0.77	17.41
YQ20	Chang 7^{1+2}	Mudstane	71.76	1.86	0.36	0.22	0.28	0.23	2.70	51.97	0.28	−3.39	8.96	−290.31	0.83	12.52
YQ21	Chang 7^{1+2}	Shale	73.42	1.45	0.62	0.12	0.38	0.44	3.51	56.34	0.56	18.08	27.68	−2.98	0.66	13.29
YQ22	Chang 7^{1+2}	Mudstane	74.52	3.83	0.73	0.38	0.41	0.15	3.14	59.22	0.33	−1.15	−3.00	−167.25	0.80	14.36
YQ23	Chang 7^{3}	Shale	78.71	9.82	4.76	0.62	2.29	0.29	4.16	70.18	1.29	82.15	32.40	368.35	0.54	23.00
YQ24	Chang 7^{3}	Shale	79.36	12.37	4.00	0.56	4.58	0.25	4.14	65.11	1.13	104.18	42.48	632.72	0.54	28.35
YQ25	Chang 7^{3}	Shale	79.95	15.61	4.12	0.58	2.51	0.23	4.08	72.48	1.47	68.98	27.48	382.72	0.54	22.48
YQ26	Chang 7^{3}	Shale	80.40	12.58	3.99	0.52	1.90	0.40	3.13	76.79	1.39	60.03	33.68	2735.27	0.57	21.71
YQ27	Chang 7^{3}	Mudstane	81.82	12.81	5.57	0.63	3.11	0.38	3.69	75.80	1.91	94.22	31.92	594.88	0.50	29.58
YQ28	Chang 7^{3}	Shale	82.36	29.50	7.71	0.75	8.62	0.48	3.17	64.32	2.28	129.47	57.92	1934.13	0.36	41.81
YQ29	Chang 7^{3}	Shale	83.02	20.84	6.36	0.69	5.80	0.35	3.44	71.18	1.96	133.91	41.76	1301.89	0.45	35.71
YQ30	Chang 7^{3}	Shale	83.49	5.01	3.05	0.44	0.89	0.34	4.94	76.70	1.32	39.05	20.60	−110.85	0.61	18.05
YQ31	Chang 7^{3}	Shale	84.49	13.03	4.90	0.44	4.53	0.32	3.87	71.82	2.61	108.84	37.24	458.86	0.39	43.98
YQ32	Chang 7^{3}	Shale	85.78	22.44	6.67	0.72	4.90	0.39	4.27	71.64	2.35	111.55	37.80	658.45	0.41	37.58
YQ33	Chang 7^{3}	Shale	86.31	29.03	9.00	0.80	8.74	0.42	3.69	65.81	3.72	137.74	43.64	845.46	0.31	60.03
YQ34	Chang 7^{3}	Shale	86.83	14.17	5.94	0.81	4.87	1.81	4.02	62.81	1.30	87.07	34.52	611.03	0.49	23.61
YQ35	Chang 7^{3}	Shale	87.41	14.43	5.96	0.82	2.63	0.46	3.03	64.71	1.04	56.99	17.64	1300.21	0.44	30.29
YQ36	Chang 7^{3}	Shale	87.97	8.01	2.91	0.63	2.20	0.27	4.11	62.66	0.87	50.05	20.20	397.55	0.61	15.50
YQ37	Chang 7^{3}	Shale	88.54	23.11	5.67	0.70	5.84	0.85	3.02	69.47	1.83	131.38	52.68	4461.52	0.42	44.33
YQ38	Chang 7^{3}	Shale	89.11	19.97	5.57	0.67	6.41	0.48	3.42	70.58	1.30	142.27	49.72	3585.83	0.45	32.15
YQ39	Chang 7^{3}	Shale	89.68	11.45	4.26	0.69	2.05	0.47	4.85	70.92	1.22	69.56	26.76	233.14	0.59	20.43
YQ40	Chang 7^{3}	Shale	90.82	24.33	7.73	0.73	7.09	0.55	3.56	74.66	2.58	148.89	52.04	2329.31	0.39	36.28
YQ41	Chang 7^{3}	Shale	91.24	11.76	4.82	0.63	3.79	0.52	3.27	72.67	1.47	92.53	37.08	1984.87	0.54	23.09
YQ42	Chang 7^{3}	Shale	91.66	18.43	5.41	0.72	4.14	0.71	3.39	63.82	1.39	107.98	39.28	3954.92	0.51	29.74
YQ43	Chang 7^{3}	Shale	92.69	5.39	2.79	0.54	1.23	0.38	4.75	63.13	0.74	63.91	29.16	253.99	0.65	14.24
YQ44	Chang 7^{3}	Mudstane	93.78	9.64	5.18	0.62	1.73	0.48	4.55	68.50	1.53	57.38	27.88	1235.32	0.51	25.57
YQ45	Chang 7^{3}	Shale	94.41	10.43	3.42	0.57	3.15	0.39	4.22	69.98	1.13	90.99	36.64	732.71	0.59	19.83
YQ46	Chang 7^{3}	Shale	95.22	13.30	4.80	0.63	3.14	0.44	4.12	71.26	1.60	87.72	33.92	724.88	0.54	21.18
YQ47	Chang 7^{3}	Shale	95.85	16.04	3.71	0.60	4.16	0.60	4.56	67.67	1.12	75.82	36.12	986.18	0.59	19.11
YQ48	Chang 7^{3}	Shale	99.56	14.46	3.54	0.56	2.48	0.45	4.71	68.12	1.18	68.86	27.36	294.04	0.56	20.98
YQ49	Chang 7^{3}	Shale	100.31	4.90	1.87	0.55	0.71	0.33	4.19	69.68	0.52	21.52	27.12	−74.32	0.76	11.08
YQ50	Chang 7^{3}	Mudstane	101.01	23.34	4.18	0.70	4.66	0.35	3.56	66.96	1.24	109.66	48.76	1407.14	0.52	24.76
YQ51	Chang 7^{3}	Shale	102.66	22.02	6.51	0.81	6.03	0.50	3.44	63.23	1.40	101.32	46.52	2482.78	0.46	33.84
YQ52	Chang 7^{3}	Mudstane	103.88	14.99	5.67	0.72	4.50	0.47	2.72	63.37	1.08	88.64	42.04	2733.56	0.54	21.05
YQ53	Chang 7^{3}	Mudstane	105.98	9.08	2.84	0.34	1.20	0.78	3.33	69.81	1.33	50.41	15.66	2856.69	0.45	26.52

Note: P1 = DOP_T; P2 = U/Th; P3 = Sr/Ba; P4 = LREE/HREE; P5 = CIA; P6 = C (Paleoclimate index); P7 = Cu_{bio}, ppm; P8 = Zn_{bio}, ppm; P9 = P_{org},ppm; P10 = Al/(Al + Fe + Mn); P11 = (Fe + Mn)/Ti.

good positive relationships between TOC and TS in both members ($R^2 > 0.65$) (Fig. 2), indicating that the enrichment of organic matter is dependent on the amount of sulphide or sulphide degree of the depositional water.

4.2. Major and trace elements

The major element data for the Chang 7 member are listed in the Supplementary data. Compared to the post-Archean average Australian shale (PAAS) (Taylor and McLennan, 1985), the Chang 7 samples demonstrated relatively low contents of SiO_2 (average = 49.35%), Al_2O_3 (average = 14.73%), and TiO_2 (average = 0.47%), but high contents of CaO (average = 2.23%) and loss on ignition (LOI, average = 18.75%). Compared with the Chang 7^{1+2} samples, the Chang 7^3 member had low contents of SiO_2 (average = 58.21% vs. 43.06%), Al_2O_3 (average = 16.42% vs. 13.53%), CaO (average = 3.39% vs. 1.41%), and TiO_2 (average = 0.57% vs. 0.39%), but high contents of Fe_2O_3 (average = 4.91% vs. 9.79%) and LOI (average = 8.90% vs. 25.74%). The high LOI values correspond to high TOC contents. The main rock-forming element concentrations ($K_2O + Na_2O$) were slightly higher in the Chang 7^{1+2} than the Chang 7^3 member, with ranges of 3.96–6.18% vs. 2.47–5.40% and averages of 4.58% vs. 3.74%, respectively. The SiO_2/Al_2O_3 ratios of the Chang 7 member varied from 2.56 to 5.21, with an average of 3.39, which is similar to that of the PAAS (Taylor and McLennan, 1985).

The chemical index of alteration (CIA) can be used to evaluate the degree of chemical weathering and represents the response to palaeoclimate during deposition. The CIA can be expressed by the following formula: CIA = molar $[Al_2O_3/(Al_2O_3 + CaO^* + Na_2O + K_2O)] \times 100$,

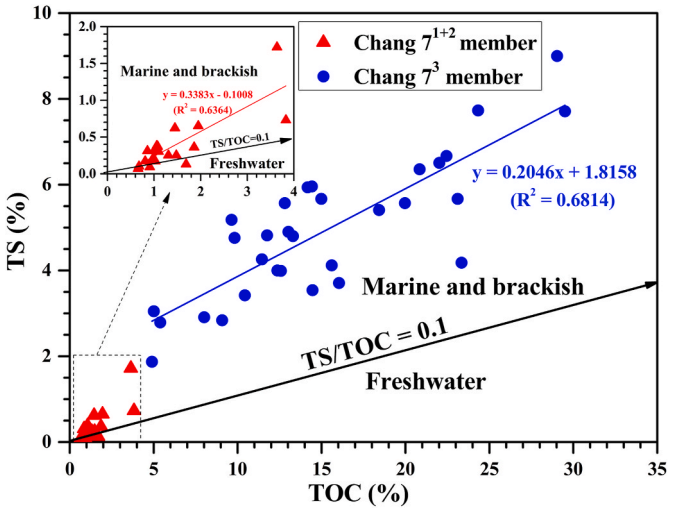

Fig. 2. TOC vs. TS in the Chang 7 member. The inset shows an expanded view of the 0–4% TOC interval (Chang 7^{1+2} member). The positive correlation of 0.1 shows the baseline value between marine, brackish water and fresh water (Wei and Algeo, 2020).

where CaO* represents the CaO from silicate minerals and can be calculated using molar CaO* = molar CaO - molar $P_2O_5 \times 10/3$ (Nesbitt and Young, 1989; McLennan, 1993). The CIA values of the Chang 7 member ranged from 51.97 to 76.79 with an average of 67.01 (Fig. 3), indicating an intermediate weathering condition and relatively warm and humid climate in the Chang 7 period (Fedo et al., 1995).

To characterise the authigenic enrichment degree of critical elements (e.g., redox-sensitive trace elements and nutrient elements related to biological growth) in samples, trace element concentrations are usually expressed in the form of enrichment factors (EFs), which are calculated by comparing the Al-normalized metal concentration to that of the PAAS. Specifically, the enrichment factor of element X (X_{EF}) is calculated according to the formula: $X_{EF} = (X/Al)_{sample}/(X/Al)_{PAAS}$, where X and Al represent the weight concentrations of elements X and Al, respectively. Enrichment factors are helpful for rapid estimation of the authigenic fraction of elements in samples. $X_{EF} > 1$ indicates the enrichment of element X compared to the PAAS concentration, $X_{EF} > 3$ represents a detectable authigenic enrichment, $X_{EF} > 10$ is considered an indication of a moderate to strong degree of authigenic enrichment, and EF < 1 indicates depleted concentration of element X relative to the standard composition (Tribovillard et al., 2006). The enrichment factors of U, Mo, Fe, P, Ba, Ni, Cu, Th, Zn, Co, and V of the Chang 7 member are shown in Fig. 4 and the Supplementary data. In the Chang 7^3 member, U and Mo were strongly enriched, P, Cu, and Co displayed detectable to moderate enrichment with a wide range of changes, and the other elements showed minor to no enrichment. However, in the Chang 7^{1+2} member, only U, Mo, Th, and Zn showed slight to moderate enrichment, while the other elements displayed depletion. Some proxies of palaeoclimate, palaeoredox, palaeosalinity, and palaeoproductivity based on trace elements are listed or shown in Table 1 and the Supplementary data, and will be discussed in detail below.

4.3. Rare earth elements

The raw data and related parameters of the REE for the Chang 7 member are listed in the Supplementary data, and the corresponding abundances of the PAAS are presented for comparison. The total REE content (including Y) ranged from 173 ppm to 323 ppm with an average of 225 ppm, which is slightly higher than that of the PAAS (212 ppm, Taylor and McLennan, 1985). The light REE (LREE) contents were

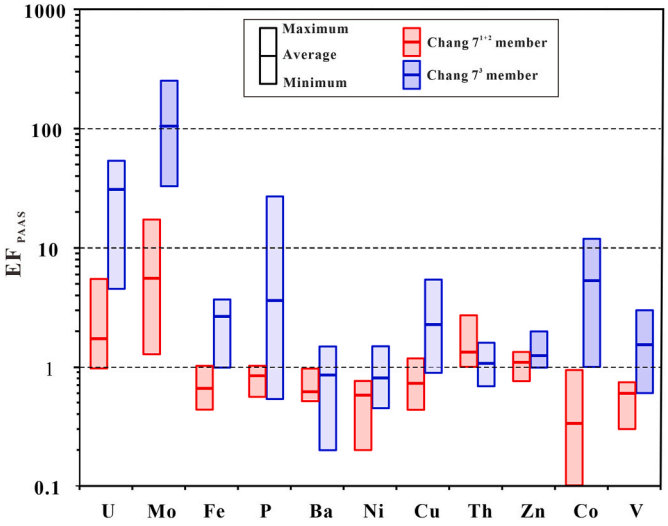

Fig. 4. Enrichment factors of some elements of the Chang 7 member.

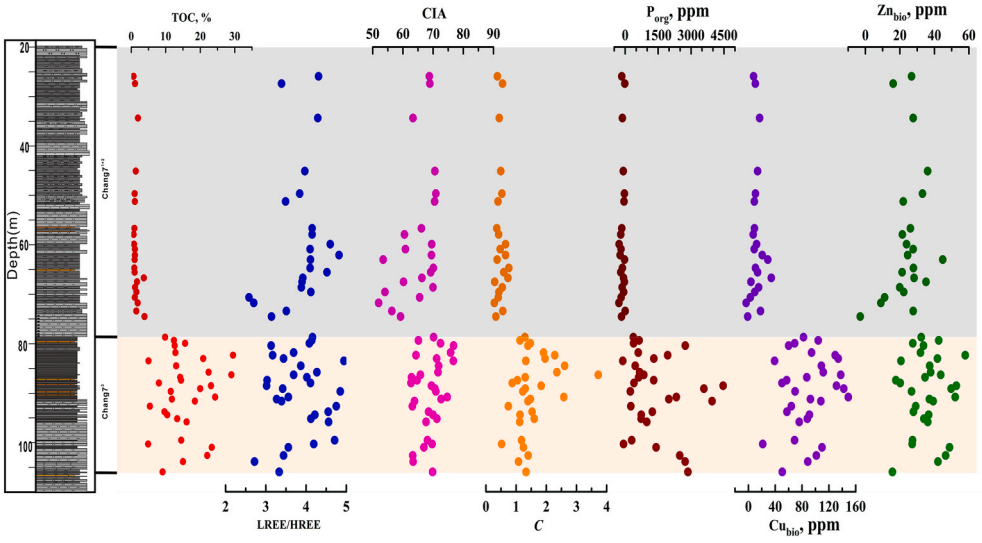

Fig. 3. Geochemical profiles and comparisons for the TOC, LREE/HREE, CIA, *C*, P_{org}, Cu_{bio}, and Zn_{bio} indicators between the Chang 7^{1+2} and Chang 7^3 members.

higher than the heavy REE (HREE) contents, with ranges of 125–245 ppm and 30–85 ppm, respectively, and the LREE/HREE ratios varied between 2.58 and 4.94 (average = 3.87), indicating that differentiation of the LREE and HREE is present in the Chang 7 member.

5. Discussion

5.1. Reconstruction of the palaeosedimentary environment

5.1.1. Redox conditions

The concentrations and enrichment factors of redox sensitive elements and their correlations are considered to be particularly useful for palaeo-environmental reconstruction (Lu et al., 2019). Mo and U are common redox-sensitive elements that are less affected by terrigenous detritus, and both appear to dissolve under oxidation conditions. U accumulates in dyoxic environments, while Mo is abundant only when H_2S appears (sulphurisation conditions), which is concurrently affected by iron manganese hydroxide. Mo–U covariant models can reflect diverse environmental information and are often used to study the redox conditions of palaeowater environments and the degree of water opening or sealing (Algeo and Tribovillard, 2009). U and Mo are generally mildly enriched in the Chang 7^{1+2} member (U_{EF} and Mo_{EF} were 1.82 and 4.88 on average, respectively), while both are strongly enriched in the Chang 7^3 shales (Fig. 4), with Mo_{EF} (average = 104.92) much higher than U_{EF} (average = 20.21). In the U_{EF}-Mo_{EF} covariant model (Fig. 5), the Chang 7^{1+2} samples ranged between 1 and 0.3 × seawater (SW) value or close to 1 × SW, showing an upward trend to the "particle shuttle" region, indicating the weakly restricted water conditions of oxidation. However, the Chang 7^3 samples showed a good positive correlation in the range of 1–3 × SW ($R^2 = 0.90$), indicating an anoxic to euxinic sulphide bottom water sedimentary environment (Tribovillard et al., 2012).

The formation of pyrite depends on the presence of H_2S in the water column or sediment pore water, yielding high pyrite mineralisation under sulphide conditions. The alternative parameter DOP_T (= 55.85/64.12 × TS/Fe_T) of Fe speciation is an effective redox evaluation index (Algeo and Liu, 2020; Algeo and Li, 2020), which has been successfully applied to modern and ancient black and organic-rich shales, such as modern Black Sea shale (Lyons, 1992), Devonian black shale of the Appalachian basin (Rimmer, 2004), and Pennsylvanian shale (Algeo and Maynard, 2008). From the published datum and documents, it can be inferred that 0.25 and 0.60 may be the safe thresholds for the DOP_T corresponding to oxic/dysoxic and dysoxic/suboxic conditions in the palaeosedimentary environment. In the southeastern margin of the Ordos Basin, the DOP_T values of most samples of the Chang 7^{1+2} member were less than 0.25, while they ranged from 0.34 to 0.82 with an average of 0.64 in the Chang 7^3 member, indicating that the water body of the Chang 7^{1+2} stage was oxidised and the Chang 7^3 strata was in an anoxic sulphide water environment.

The P cycle in the depositional system is controlled by the redox conditions of the bottom water. The oxidation condition is beneficial to the preservation of P rather than organic matter, while the opposite is the case for the reduction environment. The ratio of C_{org}/P was proposed as an index to identify redox conditions in a palaeoenvironment, with a high ratio indicating an increase in reducibility. Algeo and Ingall (2007) concluded that the ratio is generally greater than 100 under anoxic conditions and can exceed 1000, while under oxic conditions it is generally less than 50, with the lowest ratio recorded less than 10. In the study area, the C_{org}/P [(TOC/12.01)/(P/30.97)] ratios ranged from 28 to 235, averaging 66, in the Chang 7^{1+2} samples and from 69 to 609, with an average of 240, in the Chang 7^3 member samples. The distribution of the Chang 7 samples on the cross-plot of DOP_T vs. C_{org}/P ratio clearly shows that the Chang 7^{1+2} member was deposited in a dyoxic-oxic water environment, while the Chang 7^3 member was under anoxic conditions (Fig. 6).

The ratios of different redox-sensitive elements have a long history as palaeo-redox indices. The principle is that one metal is more easily enriched in sediments than the other in a certain environment (Algeo and Liu, 2020). U/Th is commonly used as this type of redox parameter, with the ratios increasing with the decrease in oxygen in the environment (Kimura and Watanabe, 2001; Rimmer, 2004). The range (average) of U/Th in the Chang 7^{1+2} samples was 0.20–0.83 (0.29), while 0.71–8.74 (3.84) in the Chang 7^3 member (Table 1). These characteristics indicate that the ancient lake was in an anoxic state in the Chang 7^3 stage, but in an oxic state during the Chang 7^{1+2} period, which is consistent with conclusions based on other redox indicess (Figs. 5 and 6).

5.1.2. Palaeosalinity

Salinity is an important hydrochemical condition that can affect the stratification of sedimentary water bodies, species, and the development of organisms, and thus affects the level of palaeoproductivity and the enrichment of organic matter in sedimentary environments (Thorpe et al., 2012; Wang et al., 2021). The ratios of Sr/Ba and TS/TOC have been widely studied and applied, and are the most reliable whole rock geochemical indicators for exploring the salinity characteristics of sedimentary palaeoenvironments (Remírez and Algeo, 2020). Wei and Algeo (2020) reported that the concentration ranges (medians) of Sr and Ba in modern marine sediments are 112–314 ppm (160 ppm) and

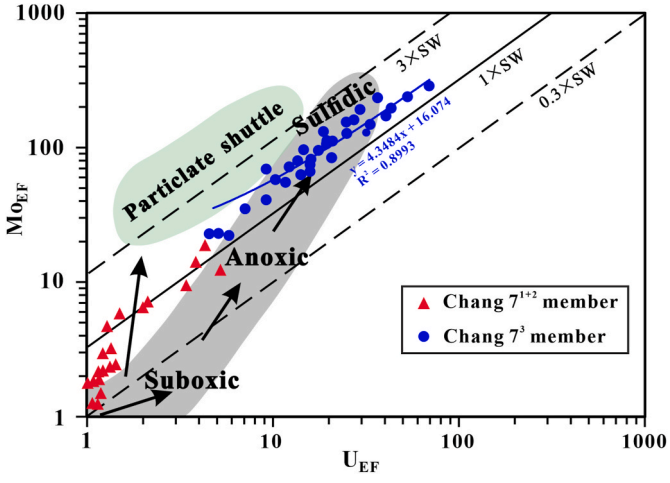

Fig. 5. U_{EF}-Mo_{EF} covariation of the Chang 7 member. The lines show that the Mo/U molar ratios are equal to the seawater value (SW). The pattern of U_{EF}-Mo_{EF} is taken from Tribovillard et al. (2009).

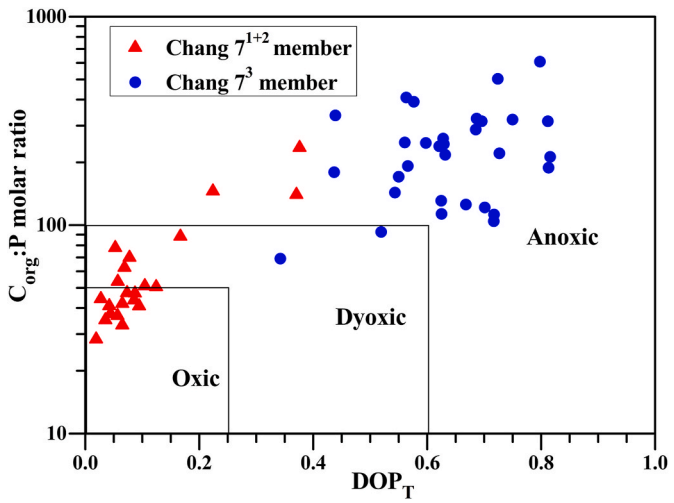

Fig. 6. C_{org}:P vs. DOP_T for the Chang 7 member. The threshold values are from Algeo and Ingall (2007) and Algeo and Liu (2020).

249–558 ppm (391 ppm), respectively, yielding Sr/Ba ratios of 0.24–0.82 (0.43). They proposed that 0.2 and 0.5 are the thresholds of Sr/Ba values to distinguish water body conditions with different salinities, that is, Sr/Ba < 0.2 indicates fresh water, 0.2–0.5 is brackish water, and >0.5 is marine water. The range of Sr/Ba in the Chang 7^{1+2} member was 0.15–0.63 (average = 0.43), while it was 0.23–0.85 (average = 0.44) in the Chang 7^3 member samples (Table 1). The concentrations of Sr and Ba in the Chang 7^{1+2} member ranged between 69–214 ppm and 290–500 ppm, with averages of 161 ppm and 379 ppm, respectively, and between 83–415 ppm and 100–770 ppm, with averages of 201 ppm and 445 ppm, respectively, in the Chang 7^3 member samples. Both show ranges that are close to the concentration range and ratio characteristics of Sr and Ba in modern marine sediments, indicating that the ancient lake was brackish water during the deposition of the Chang 7 member on the southeastern margin of the Ordos Basin. The majority of these samples fall in the field of brackish water sedimentary environment in the Sr vs. Ba diagram (Fig. 7), corresponding to the palaeoenvironment and salinity information indicated by the relationship between TS and TOC in the samples (Fig. 2) (Wei and Algeo, 2020). The Ordos Basin evolved into an inland basin in the middle-late Early Triassic (Yang et al., 2005; Qiu et al., 2014). The brackish marine environment indicated in Figs. 2 and 7 may be related to seawater intrusion (Wang et al., 2017) or event deposition, such as volcanic and hydrothermal activities (Zhang et al., 2020; Ji et al., 2021), during the deposition of the Chang 7 member in the southeastern margin of the Ordos Basin. However, further evidence is required to confirm this hypothesis, which requires further study.

5.1.3. Deposition rate

The sedimentation rate determines the retention time of sediments in water, which is considered to be one of the main factors controlling organic matter enrichment in shale (Tyson, 2001; Chen et al., 2019). Organic matter in sediments generally increases with increasing sedimentation rate. However, a sedimentation rate that is too fast or too slow is not conducive to the enrichment of organic matter. Too high sedimentation rates lead to organic matter dilution, while too low sedimentation rates increase the probability of degradation of organic matter during oxidation (Ding et al., 2015).

The degree of REE differentiation is considered to be a response to variations in the sedimentation rates. REEs are gradually deposited by combining with detrital minerals or in the form of suspended fine particles in water. If the sedimentation rate is low, REEs have sufficient time to be absorbed by clay fragments or to react with organic matter, resulting in LREE enrichment and HREE depletion, and the fractionation degrees of LREE and HREE are low; if the sedimentation rate is high, the opposite is true (Johannesson et al., 1994). The LREE/HREE, $(La/Sm)_N$, and $(Gd/Yb)_N$ (N = PAAS normalized, Taylor and McLennan, 1985) ratios can be used to characterise the degree of differentiation of the REEs, LREEs, and HREEs, respectively (McLennan et al., 1995; Chen et al., 2019). In this study, these parameters were relatively stable in the different members, ranging from 2.58 to 4.94, 0.71 to 1.06, and 0.77 to 1.51, with averages of 3.87, 0.88, and 1.23, respectively. These data show that the LREEs were enriched and the HREEs depleted and fractionated, while there were no obvious element differentiations in the LREE, indicating that the sedimentation rates may have been relatively high when the Chang 7 member was deposited.

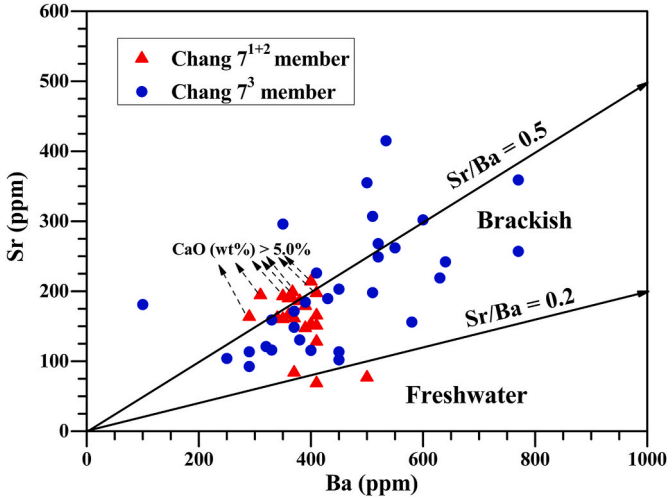

Fig. 7. Ba vs. Sr (ppm), indicating the palaeosalinity of the Chang 7 member. The general pattern is based on Wei and Algeo (2020). Samples with CaO content greater than 5.0% are marked, which may be affected by carbonate-hosted Sr.

5.2. Evaluation of palaeoproductivity

5.2.1. Palaeoclimate

The palaeoclimate controlled the amount of sunshine, humidity and weathering degree, dominated the supply of sediment sources and the composition and quantity of biological species, and thus affected the palaeoproductivity in the sedimentary system (Chen et al., 2020). Owing to the difference in the chemical stabilities of major oxides, the plots of SiO_2 vs. $(Al_2O_3 + K_2O + Na_2O)$ and Ga/Rb vs. K_2O/Al_2O_3 were used to estimate the palaeoclimate characteristics of the sedimentary rock formation period (Roy and Roser, 2013). Almost all sampling locations were humid climate regions in the charts (Fig. 8), and their significance is consistent with the CIA characteristics (Fig. 3).

The migration and distribution laws of the elements of the humid

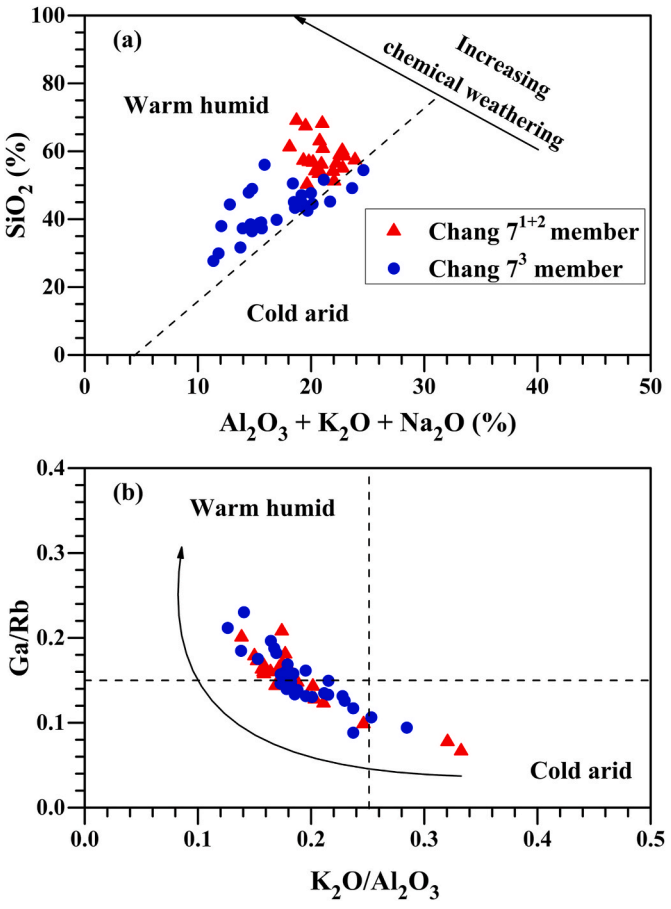

Fig. 8. Plots of (a) SiO_2 vs. $(Al_2O_3 + K_2O + Na_2O)$ (%) and (b) Ga/Rb vs. K_2O/Al_2O_3, indicating the palaepclimate of the Chang 7 member.

climate type (Fe, Mn, Cr, V, Co, and Ni) and the dry climate type (Ca, Mg, K, Na, Sr, and Ba) are closely related to the palaeoclimate. The ratio of these two kinds of elements was defined as the palaeoclimate index (*C*) and is used to characterise climate change, with high values indicating warm and humid climates (Guan, 1992; Li et al., 2020). The values of *C* ranged from 0.28 to 0.76 (average of 0.48) in the Chang 7^{1+2} member and from 0.52 to 3.72 (average of 1.53) in the Chang 7^3 member (Fig. 3), suggesting that the palaeoclimate in the early stage was warmer and wetter than that in the middle-late stage of the Chang 7 period.

The Sr/Cu ratio is another commonly used parameter sensitive to palaeoclimate change: low ratios indicate warm and humid climates (Tribovillard et al., 2006). Ratios ranging between 1.3 and 5.0 indicate a humid and warm climate, while ratios >5 indicate that the climate is mainly arid and hot (Li et al., 2020). The average Sr/Cu was 4.59 (range 2.14–6.70) in the Chang 7^{1+2} member and 2.05 (range 0.69–6.03) in the Chang 7^3 member samples, indicating that the study area was warm and humid in the Chang 7 period and that it was warmer and wetter in the early stage. These results were consistent with the results of the palaeoclimatic indicator *C*.

5.2.2. Productivity

The abundance of specific trace elements in sediments has been employed to evaluate or reconstruct the primary productivity of sedimentary systems (Tribovillard et al., 2006). However, only the elements related to biogenesis were found to be reliable. Therefore, the effect of terrigenous detritus input should be deducted, which is particularly important for terrestrial environments such as lakes. Al has been used as an indicator of terrigenous input because it is mainly derived from terrigenous detritus with stable chemical properties and very low solubility in water. The formula used in this study to deduct terrigenous inputs is: E_{org} or $E_{bio} = E_{sample} - Al_{sample} \times (E/Al)_{detr}$, where E_{org} or E_{bio} is the organic or biogenic part of the elements, with negative values indicating that the material is mainly from terrigenous detritus; E_{sample} and Al_{sample} are the abundances of the elements E and Al in the samples, respectively; and $(E/Al)_{detr}$ is the ratio of the average abundance of E and Al in the upper continental crust (McLennan, 2001). The $(P/Al)_{detr}$, $(Cu/Al)_{detr}$, $(Zn/Al)_{detr}$, and $(Ba/Al)_{detr}$ are 0.0087, 0.0003, 0.0008, and 0.0065, respectively (Shen et al., 2015; Schoepfer et al., 2015; Gao et al., 2018).

P is a key nutrient for the growth of organisms. Its enrichment is one of the commonly used indicators for the primary productivity and has been widely used in the evaluation of modern and ancient productivity, but the redox conditions of the water body should also be considered in the interpretation of this index (Algeo and Ingall, 2007). The P_{org} of the Chang 7^{1+2} samples were negative, indicating that P was mainly derived from terrigenous input. Although P_{org} may be underestimated due to recycling into the water under reducing conditions (Kraal et al., 2012), the majority of the Chang 7^3 samples had positive P_{org} values, ranging from −110.85 ppm to 4461.52 ppm and averaging 1364.30 ppm (Table 1), with some values even higher than those in modern ocean with high productivity of the upwelling current region (rangeing from 100 to 19,000 ppm, with an average of 2700 ppm, n = 27, Murray and Leinen, 1993). This indicates that the palaeolake had a relatively high primary productivity during the deposition of the Chang 7^3 member.

With photosynthesis of the primary producers in the water body, Cu and Zn are absorbed by organisms to form their own organic matter and thus preserved in sediments with their deposition (Tribovillard et al., 2006). The abundance of Cu and Zn in sediments is closely related to the deposition of organic matter, which is used to quantitatively characterise the primary productivity of palaeowater (Piper and Perkins, 2004). This approach is especially suitable for investigating the change in productivity under reducing conditions due to the need to form sulphides for preservation. Calculated Cu_{bio} values are normally elevated in highly productive zones near the equator of the modern ocean, ranging from 1.32 ppm to 53.10 ppm (average = 24.9 ppm, n = 15, Murray and Leinen, 1993). The ranges of Cu_{bio} in the Chang 7^{1+2} and 7^3 samples ranged from −3.39 ppm to 34.10 ppm (average = 11.73 ppm) and from 21.52 ppm to 148.89 ppm (average = 89.45 ppm), respectively, indicating that the primary productivity of the palaeolake was high during the Chang 7^3 period, but noticeably decreased in the Chang 7^{1+2} stage (Fig. 3). The abundance of Zn showed similar characteristics. The Zn_{bio} values ranged from −3.00 ppm to 44.80 ppm and 15.66 ppm–57.92 ppm in the Chang 7^{1+2} and 7^3 samples, with averages of 24.06 ppm and 35.74 ppm, respectively, suggesting that the Chang 7^3 member had high palaeoproductivity (Fig. 3).

Biogenic Ba (Ba_{bio}) mainly exists in the form of barite, which is unstable and dissolves in strong sulphurisation environments, depleting it in the sediments (Vanos et al., 1991). Therefore, the influence of the redox conditions of bottom water should be considered when using Ba_{bio} to estimate palaeoproductivity characteristics (Dehairs et al., 1992). The Ba_{bio} values of the Chang 7^{1+2} member were mainly negative, which can be interpreted as low palaeoproductivity levels and Ba as mainly terrigenous input. However, considering the high values of P_{org}, Cu_{bio}, and Zn_{bio}, the negative values of Ba_{bio} in some samples of the Chang 7^3 member (ranging from −310.15 ppm to 254.30 ppm, averaging −0.88 ppm) may be influenced by the loss of Ba_{bio} in the sulphide-reducing environment of the Chang 7^3 member.

5.2.3. Event deposition

Event deposition, such as volcanic and hydrothermal activity, can often disrupt the balance of the original lake ecosystem and affect the enrichment of organic matter (Zhang et al., 2020). The existence of volcanic and hydrothermal activities in the Yangchang Formation in the Ordos Basin has been confirmed by previous studies using different methods, such as major and trace elements (He et al., 2016), the mineral assemblage of hematite–pyrite–anhydrite and $\delta^{34}S$ values (Liao et al., 2019), and PGEs and REEs (Qiu et al., 2015). In the core samples of the Chang 7 member in this study, thin or laminar tuffs and tuffaceous mudstones are well developed. The tuffs are yellow and can be easily distinguished from siliceous clastic sediments, while the tuffaceous mudstones are mostly grey massive mudstones with a high abundance of REEs (Fig. S1), indicating volcanic activity during the deposition of the Chang 7 member in the study area (Qiu et al., 2014).

In sedimentary rocks, Al and Ti are excellent indicators of terrigenous input, while Fe and Mn are usually enriched in hydrothermal deposits and can be used to indicate the presence of hydrothermal sedimentation (Murray, 1994; Li et al., 2014). The ratios of (Fe + Mn)/Ti and Al/(Al + Fe + Mn) in typical hydrothermal sediments are usually greater than 15 and less than 0.4, respectively. The Al/(Al + Fe + Mn) ratio is also a valid parameter for evaluating the contribution or influence of hydrothermal sedimentary components in sediments. The ratio increases with increasing terrigenous input or decreasing hydrothermal influence; in contrast, the ratio decreases with increasing hydrothermal sedimentary input or influence (He et al., 2016). The (Fe + Mn)/Ti and Al/(Al + Fe + Mn) ratios of the Chang 7 member samples ranged from 6.82 to 60.02 and 0.31 to 0.83, with averages of 20.40 and 0.60, respectively. A minority of these samples, mainly from the Chang 7^3 member, was hydrothermal sediments (Fig. 9), suggesting that hydrothermal activity did affect the study area, but that there was a relatively high component of terrigenous input in the sediments. The Y_N/Ho_N ratios, ranging from 0.92 to 1.12, also indicate that some samples had hydrothermal input and influence (Bau et al., 2014). The enrichment of P, Fe, U, Mo, Cu, V, and Co in the Chang 7^3 member samples may be related to volcanic activity or hydrothermal fluids (Fig. 4).

5.3. Enrichment mechanism of organic matter

Organic matter accumulation in fine-grained sedimentary rocks generally occurs via three different models, based on productivity, preservation, or sedimentation rate (Tyson, 2001, 2005; Katz, 2005). However, organic matter enrichment depends on various factors related to biosynthesis, biological productivity, organic carbon flux, physical

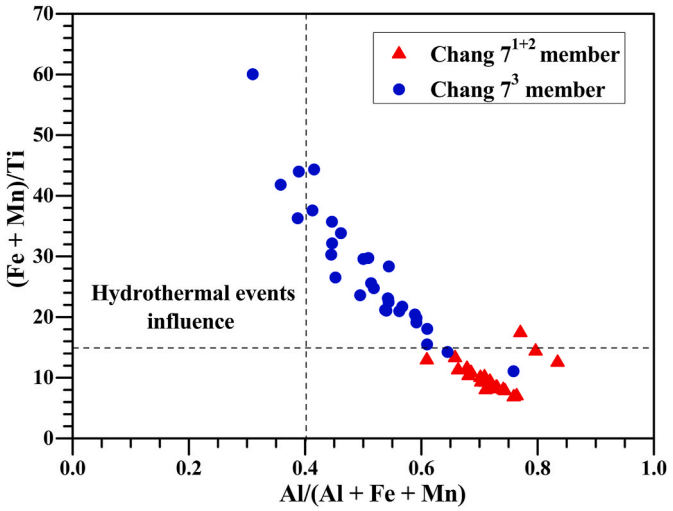

Fig. 9. (Fe + Mn)/Ti vs. Al/(Al + Fe + Mn), indicating the influence of hydrothermal activity on the Chang 7 member.

weathering and transportation processes, bottom water oxygen concentration, and geochemical exchange processes during and after deposition. None of these factors alone control the enrichment of organic matter independently and absolutely. Instead, high abundances of organic matter in black shale are usually the result of a combination of multiple favourable factors or models.

In this study, a parameter dataset comprising 11 elemental proxies related to reconstruction or evaluation of the depositional environment and palaeoproductivity was processed by PCA to gain insights into organic matter enrichment. The C_{org}:P molar ratio proxy calculated in TOC for the redox conditions was excluded from the dataset to avoid a mutual influence. The obtained PCA scores and loadings were used to explore the samples and parameters (Fig. 10). The first three PCs accounted for 81.65% (PC1, PC2, and PC3 = 59.88%, 12.19%, and 9.58%, respectively) of the total variance in the original dataset. Only 18.36% of the variance was not represented. In the 2D-PCA plot (Fig. 10a), all data points of the Chang 7^{1+2} member are located on the left of PC1 = 0, while most of the Chang 7^3 samples are on the right. The TOC values of all the samples and PC1 scores showed an excellent linear correlation (R^2 = 0.92, Fig. 11), while there were poor correlations between the TOC values and PC2 and PC3 scores (R^2 < 0.01, Fig. 11). This suggests that the enrichment of organic matter in the Chang 7 member may have been primarily controlled by the intrinsic attributes of PC1.

To comprehend the main representative significance of the most important PC, the relative contributions of each variable (parameter), namely loading, related to PC1, PC2, and PC3 were investigated. In general, parameters with larger absolute loading values represent the main features of the relevant PC. Fig. 10b shows the loading plot based on the first three PCs vs. the 11 geochemical proxies used in PCA. The loadings on PC2 are dominated by a positive correlation with the LREE/HREE ratio, which is an index of the deposition rate (Johannesson et al., 1994). The loadings on PC3 mainly show a positive correlation with the Sr/Ba ratio, a salinity proxy of the sedimentary water body (Wei and Algeo, 2020). Thus, PC2 could be interpreted as an indicator of the deposition rate, whereas PC3 could be used to characterise the salinity of the sedimentary environment. According to the correlations between the TOC content of the samples and the first three PCs (Fig. 11), the sedimentation rate and salinity of the depositional environment may not be the main factors controlling the enrichment of organic matter in the Chang 7 member.

The loadings on PC1 are dominated by a positive correlation with multiple parameters, including Cu_{bio}, U/Th, (Fe + Mn)/Ti, *C*, and DOP_T with loading values > 0.33 that decreased in turn, and were negatively

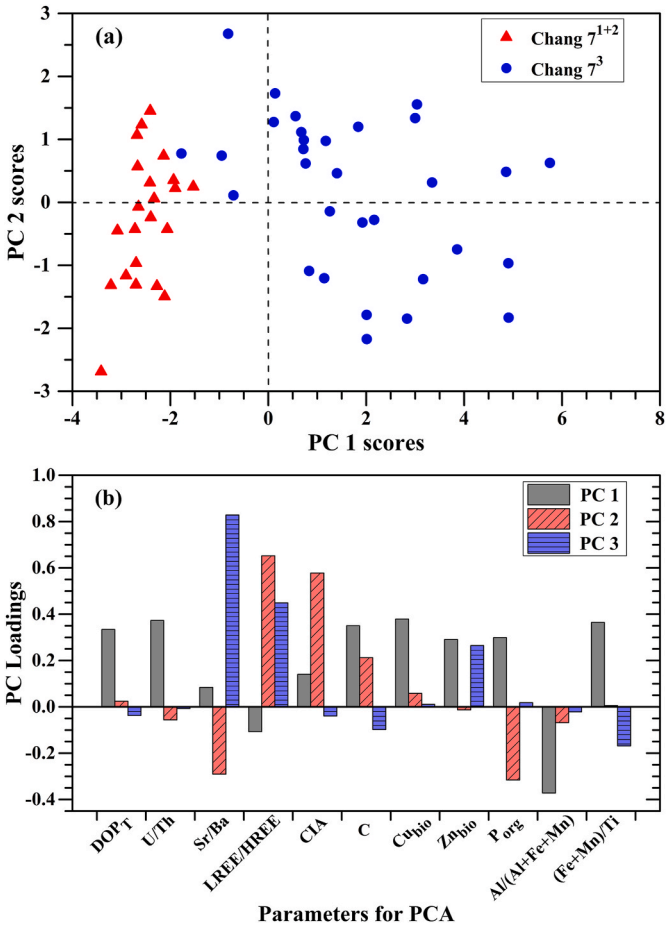

Fig. 10. PCA results: (a) Distribution of the Chang 7 samples of the PC1 vs. PC2 scores (2D-PCA plot); (b) Loading plot of the first three PCs vs. the 12 geochemical proxies used in PCA.

correlated with the Al/(Al + Fe + Mn) ratio (Fig. 10). Cu_{bio} is an indicator of palaeoproductivity (Piper and Perkins, 2004), and its loading reached 0.38. The loadings of the other two palaeoproductivity proxies, P_{org} and Zn_{bio} (Algeo and Ingall, 2007), reached 0.30 and 0.29, respectively. The (Fe + Mn)/Ti and Al/(Al + Fe + Mn) ratios are indicators of hydrothermal activity (Li et al., 2014). The former increases with hydrothermal activity, while the latter shows the opposite trend. Hydrothermal fluids containing a large amount of material, such as P, Fe, Mn, Cu, and other nutrient elements, enter the surface of the sedimentary water body through upwelling, which promotes the flourishing of organisms (mainly algae), improves the initial productivity, and provides sufficient organic matter sources for accumulation (Zhang et al., 2020). A large amount of reducing gases (e.g., H_2S and CO) released along with hydrothermal activities can easily lead to the formation of anoxic and euxinic conditions in bottom waters, which is conducive to the preservation of organic matter (Wille et al., 2008). *C* is a palaeoclimate proxy that increases with the warmth and humidity of a climate (Li et al., 2020). Warm humid climates have increased weathering intensity, which is always accompanied by large inputs of nutrient elements for primary producers and terrigenous detrital matter. The former promotes palaeoproductivity mainly by promoting algal growth or blooms and the latter provides sufficient medium for the adsorption and deposition of organic matter, whereas excessive input of terrigenous material leads to dilution of organic matter (Li et al., 2017). The linear relationships between Cu_{bio} and (Fe + Mn)/Ti, Al/(Al + Fe + Mn), and *C* indicate that hydrothermal activity and warm humid climate can improve palaeoproductivity (Fig. S2). U/Th and DOP_T are effective redox evaluation indices (Rimmer, 2004; Algeo and Li, 2020), whose

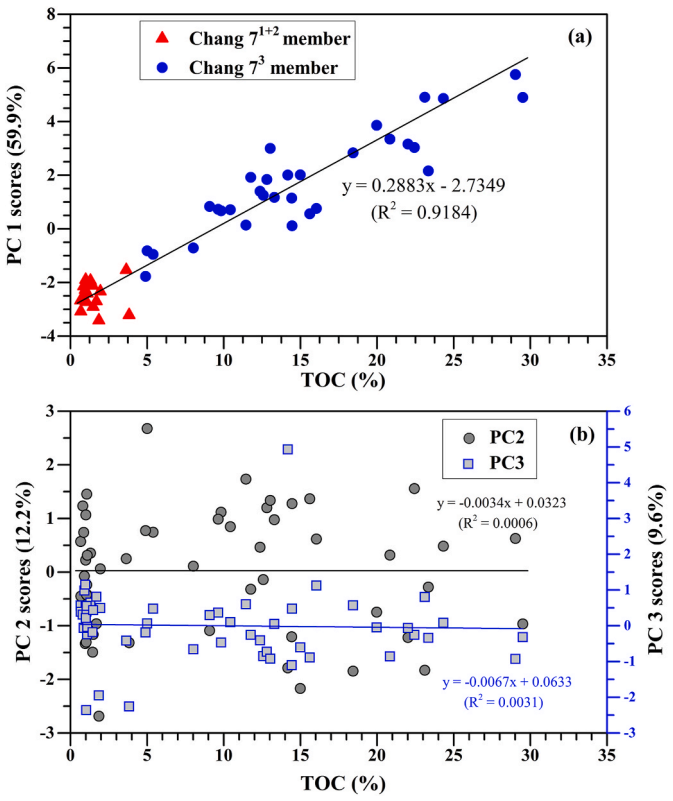

Fig. 11. Relationships of TOC and the first three PC scores: (a) TOC vs. PC1, and (b) TOC vs PC2 and PC3.

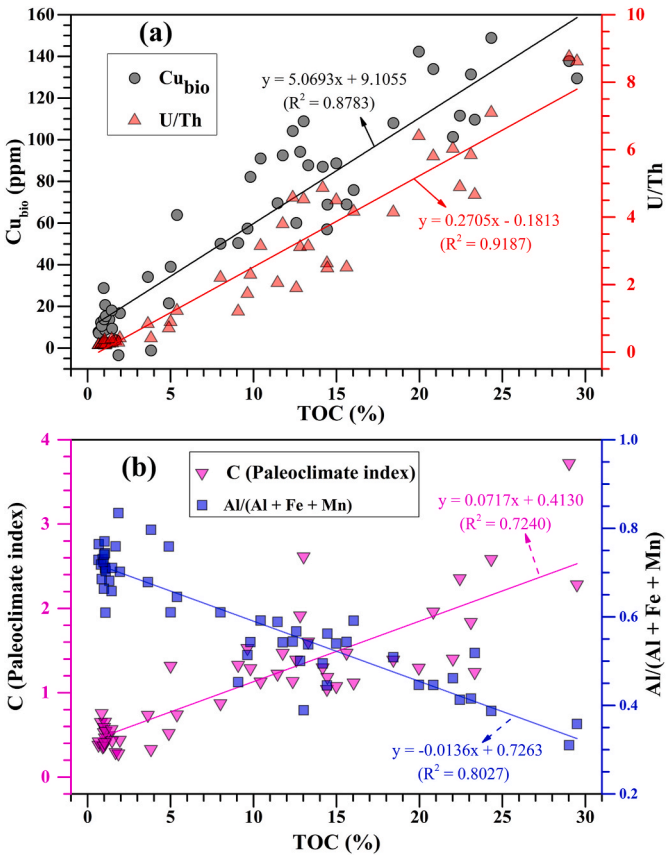

Fig. 12. Relationships of TOC (%) and some geochemical proxies. (a) TOC vs. Cu (ppm) and U/Th, and (b) TOC vs. *C* and Al/(Al + Fe + Mn).

values increase with increasing reducibility of the depositional environment, and their loadings on PC1 reached 0.37, and 0.33, respectively. Although there are several factors affecting PC1 according to the absolute loading values of the parameters, it can be concluded that PC1 mainly represents the characteristics of palaeoproductivity and redox conditions and can be interpreted as an indicator of these factors.

Therefore, the enrichment of organic matter in the Chang 7 member was mainly controlled by palaeoproductivity and the preservation environment based on the excellent positive linear correlations between the TOC content of the samples and the PC1 scores (Fig. 11a). This inference can also be confirmed by the linear relationship between TOC and the parameters of the Chang 7 samples. For example, there are similar trends in TOC and the palaeoproductivity proxies (Fig. 3) and good positive linear relationships between TOC and Cu_{bio} and U/Th (R^2 = 0.88 and 0.92, respectively, Fig. 12a), suggesting that elevated primary palaeoproductivity and enhanced preservation related to anoxia correspond to high TOC. Similarly, TOC is linearly related with the Al/(Al + Fe + Mn) ratio and palaeoclimate index C (Fig. 12b), indicating that hydrothermal activity and a warm humid palaeoclimate enhanced the enrichment of organic matter during the deposition of the Chang 7 member.

The difference in TOC between the Chang 7^{1+2} and 7^3 samples is due to the differences in palaeoproductivity and redox conditions between the two members. In the early period of the Chang 7^3 member, a lake-bottom hydrothermal fluid and frequent volcanic activities existed on the southern margin of the Ordos Basin (Zhang et al., 2020). The warm humid palaeoclimate increased the weathering intensity resulting in large inputs of nutrient elements for primary producers and terrigenous detrital matter for the adsorption and deposition of organic matter. The nutrient element and Fe-rich volcanic ash and hydrothermal fluids were carried to the surface of the lake in large quantities, which promoted the flourishing of algae and bacteria and provided sufficient organic matter sources for accumulation. The upwelling and mixing of hydrothermal fluids may have led to an increase in salinity and stratification of the water column, conducive to the preservation of organic matter. Reducing gases released with hydrothermal activity contributed to the formation of an extremely anoxic and H_2S-rich sedimentary environment at the bottom of the lake, which enhanced the enrichment of redox-sensitive elements and the preservation of buried organic matter. Thus, it can be concluded that the high palaeoproduction and superior preservation conditions related to event deposition and the warm and humid palaeoclimate were the potential mechanisms for the formation of high-quality source rocks and oil shale in the Chang 7^3 member. However, in the middle-late period of the Chang 7^{1+2} member, volcanic and hydrothermal activities were weak, lacustrine organisms began to decrease, and the sedimentary environment transformed to an oxidation environment, resulting in the decline of productivity and organic matter preservation conditions of the ancient lake, which reduced the enrichment and preservation of organic matter and led to low TOC values.

6. Conclusions

The lacustrine black shales of the Chang 7 member of the upper Triassic Yanchang Formation are the main source rocks and the most important unconventional (shale oil) petroleum resources in the Ordos Basin. The TOC and TS contents of the Chang 7^3 member were found to be higher than those of the Chang 7^{1+2} member, with averages of 15.24% and 4.93% vs. 1.39% and 0.37%, respectively. The parameters related to the palaeoredox, such as the Mo_{EF}-U_{EF} covariant and the values of DOP_T, C_{org}/P, and U/Th, indicate that the ancient lake was dyoxic-oxic during the Chang 7^{1+2} period, while it had anoxic to euxinic sulphide bottom water in the Chang 7^3 period. The abundances and relationships of TOC & TS and Sr & Ba indicate that the ancient lake was a brackish water body during the deposition of the Chang 7 member.

Enrichment of LREEs and fractionation of HREEs show that the sedimentation rate was relatively high when the Chang 7 member was deposited. The values of CIA, *C*, and Sr/Cu demonstrate that the palaeoclimate in the early stage was warmer and wetter than that in the middle-late stage in the Chang 7 period. The evaluation proxies of palaeoproductivity, P_{org}, Cu_{bio}, and Zn_{bio}, suggest that the palaeolake had a relatively high primary productivity during the deposition of the Chang 7^3 member, while it was decreased in the Chang 7^{1+2} period. The development of thin or laminar tuffs and tuffaceous mudstones and the enrichment in Fe, Mn, and other elements demonstrate that the Chang 7 member was influenced by event deposition, such as volcanic and hydrothermal activities.

The elemental geochemical data were combined with chemometric analysis to gain insights into organic matter enrichment. A parameter dataset comprising 11 elemental proxies related to reconstruction or evaluation of the depositional environment and palaeoproductivity was processed by PCA. The first three PCs (PC1, PC2, and PC3) were found to account for 81.64% of the total variance in the original dataset. The TOC values of the Chang 7 samples and PC1 scores showed an excellent linear correlation, while there were poor correlations between the TOC values and PC2 and PC3 scores. PC1 mainly represents the characteristics of palaeoproductivity and redox conditions and can be interpreted as an indicator of those factors, while PC2 and PC3 could be used to characterise the deposition rate and the salinity of sedimentary environment, respectively. Therefore, the enrichment of organic matter of the Chang 7 member was mainly controlled by palaeoproductivity and the preservation environment. The combination of PCA and element geochemistry allows detailed paleoenvironmental inferences and organic matter enrichment. The practical application of this work can serve as a model for other studies.

Declaration of competing interest

We declared that we have no conflicts of interest to this work.

Acknowledgements

We appreciate Dr. Thomas Algeo, another anonymous reviewer and Dr. Jinqiang Tian for their comments. We thank Drs. Yao-Ping Wang and Xiao-Hui Lin for the help to this study. This work was supported by the Natural Science Foundation of China (Grant No. 41621062) and the State Key Laboratory of Organic Geochemistry Project (Grant No. SKLOG2020–1). This is contribution No. IS–3093 from GIGCAS.

Appendix A. Supplementary data

Supplementary data to this article can be found online at https://doi.org/10.1016/j.marpetgeo.2021.105404.

References

Algeo, T.J., Maynard, J.B., 2004. Trace-element behavior and redox facies in core shales of Upper Pennsylvanian Kansas-type cyclothems. Chem. Geol. 206 (3–4), 289–318.
Algeo, T.J., Ingall, E., 2007. Sedimentary Corg: P ratios, paleocean ventilation, and Phanerozoic atmospheric pO_2. Palaeogeogr. Palaeoclimatol. Palaeoecol. 256, 130–155.
Algeo, T.J., Maynard, J.B., 2008. Trace metal covariation as a guide to water-mass conditions in ancient anoxic marine environments. Geosphere 4 (5), 872–887.
Algeo, T.J., Tribovillard, N., 2009. Environmental analysis of paleoceanographic systems based on molybdenum–uranium covariation. Chem. Geol. 268 (3), 211–225.
Algeo, T.J., Li, C., 2020. Redox classification and calibration of redox thresholds in sedimentary systems. Geochem. Cosmochim. Acta 287, 8–26.
Algeo, T.J., Liu, J., 2020. A re-assessment of elemental proxies for paleoredox analysis. Chem. Geol. 540, 119549.
Bau, M., Schmidt, K., Koschinsky, A., Hein, J., Kuhn, T., Usui, A., 2014. Discriminating between different genetic types of marine ferro-manganese crusts and nodules based on rare earth elements and yttrium. Chem. Geol. 381, 1–9.
Chen, G., Gang, W., Liu, Y., Wang, N., Guo, Y., Zhu, C., Cao, Q., 2019. High-resolution sediment accumulation rate determined by cyclostratigraphy and its impact on the organic matter abundance of the hydrocarbon source rock in the Yanchang Formation, Ordos Basin, China. Mar. Petrol. Geol. 103, 1–11.
Chen, G., Gang, W., Chang, X., Wang, N., Zhang, P., Cao, Q., Xu, J., 2020. Paleoproductivity of the Chang 7 unit in the Ordos Basin (north China) and its controlling factors. Palaeogeogr. Palaeoclimatol. Palaeoecol. 551, 1–13.
Demaison, G.T., Moore, G.T., 1980. Anoxic environments and oil source bed genesis. Org. Geochem. 2, 9–31.
Dehairs, F., Baeyens, W., Goeyens, L., 1992. Accumulation of suspended barite at mesopelagic depths and export production in the Southern Ocean. Science 258, 1332–1335.
Ding, X., Liu, G., Zha, M., Huang, Z., Gao, C., Lu, X., Sun, M., Chen, Z., Liuzhuang, X., 2015. Relationship between total organic carbon content and sedimentation rate in ancient lacustrine sediments, a case study of Erlian Basin, northern China. J. Geochem. Explor. 149, 22–29.
Fedo, C.M., Nesbitt, H.W., Young, G.M., 1995. Unraveling the effects of potassium metasomatism in sedimentary rocks and paleosols, with implications for paleoweathering conditions and provenance. Geology 23 (10), 921–924.
Gao, P., He, Z., Li, S., Lash, G.G., Li, B., Huang, B., Yan, D., 2018. Volcanic and hydrothermal activities recorded in phosphate nodules from the Lower Cambrian Niutitang Formation black shales in South China. Palaeogeogr. Palaeoclimatol. Palaeoecol. 505, 381–397.
Guan, Y., 1992. The elements, clay minerals and sedimentary environment of Horqin sand land. J. Desert Res. 12 (1), 9–15 (in Chinese with English abstract).
He, C., Ji, L., Wu, Y., Su, A., Zhang, M., 2016. Characteristics of hydrothermal sedimentation process in the Yanchang Formation, south Ordos Basin, China: evidence from element geochemistry. Sediment. Geol. 345, 33–41.
Ibach, L.E.J., 1982. Relationship between sedimentation rate and total organic carbon content in ancient marine sediments. AAPG Bull. 66, 170–188.
Ji, L., Li, J., Zhang, M., Lu, H., He, C., Jin, P., Ma, B., 2021. Effects of lacustrine hydrothermal activity on the organic matter input of source rocks during the Yanchang period in the Ordos Basin. Mar. Petrol. Geol. 125, 104868.
Johannesson, K.H., Lyons, W.B., Bird, D.A., 1994. Rare earth element concentrations and speciation in alkaline lakes from the western. U.S.A. Geophys. Res. Lett. 21 (9), 773–776.
Katz, B.J., 2005. Controlling factors on source rock development-a review of productivity, preservation, and sedimentation rate. Soc. Sediment. Geol. 82, 7–16.
Kimura, H., Watanabe, Y., 2001. Oceanic anoxia at the Precambrian-Cambrian boundary. Geology 29 (11), 995–998.
Kraal, P., Slomp, C.P., Reed, D.C., Reichart, G.J., Poulton, S.W., 2012. Sedimentary phosphorus and iron cycling in and below the oxygen minimum zone of the northern Arabian Sea. Biogeosciences 9 (7), 2603–2624.
Lash, G.G., Blood, D.R., 2014. Organic matter accumulation, redox, and diagenetic history of the Marcellus Formation, southwestern Pennsylvania, Appalachian basin. Mar. Petrol. Geol. 57, 244–263.
Li, H., Zhai, M., Zhang, L., Gao, L., Yang, J., Zhou, Y., He, J., Liang, J., Zhou, L., Voudouris, P.C., 2014. Distribution, microfabric, and geochemical characteristics of siliceous rocks in central orogenic belt, China: implications for a hydrothermal sedimentation model. Sci. World J. 780910.
Li, W., Lu, S., Tan, Z., He, T., 2017. Lacustrine source rock deposition in response to coevolution of the paleoenvironment and formation mechanism of organic-rich shales in the Biyang depression. Nanxiang Basin. Energ. Fuel 31, 13519–13527.
Li, X., Gang, W., Yao, J., Gao, G., Wang, C., Li, J., Liu, Y., Guo, Y., Yang, S., 2020. Major and trace elements as indicators for organic matter enrichment of marine carbonate rocks: a case study of Ordovician subsalt marine formations in the central-eastern Ordos Basin, North China. Mar. Petrol. Geol. 111, 461–475.
Liao, S., Tao, C., Zhu, C., Li, H., Li, X., Liang, J., Yang, W., Wang, Y., 2019. Two episodes of sulfide mineralization at the Yuhuang-1 hydrothermal field on the Southwest Indian Ridge: insight from Zn isotopes. Chem. Geol. 507, 54–63.
Lu, Y., Jiang, S., Lu, Y., Xu, S., Wang, Y., 2019. Productivity or preservation? the factors controlling the organic matter accumulation in the late katian through Hirnantian Wufeng organic-rich shale, south China. Mar. Petrol. Geol. 109, 22–35.
Lyons, T.W., 1992. Comparative Study of Holocene Black Sea Sediments from Oxic and Anoxic Sites of Deposition: Geochemical and Sedimentological Criteria. Ph.D. dissertation. Yale Univ., New Haven, Conn., p. 377
McLennan, S.M., 1993. Weathering and global denudation. J. Geol. 101, 295–303.
McLennan, S.M., 2001. Relationship between the trace element composition of sedimentary rocks and upper continental crust. G-cubed 2 (4), 203–236.
McLennan, S.M., Hemming, S.R., Taylor, S.R., Eriksson, K.A., 1995. Early Proterozoic crustal evolution: geochemical and NdPb isotopic evidence from metasedimentary rocks, southwestern North America. Geochem. Cosmochim. Acta 59 (6), 1153–1177.
Murray, R.W., 1994. Chemical-criteria to identify the depositional environment of chert-general-principles and applications. Sediment. Geol. 90, 213–232.
Murray, R.W., Leinen, M., 1993. Chemical transport to the seafloor of the equatorial Pacific Ocean across a latitudinal transect at 135°W: tracking sedimentary major, trace, and rare earth element fluxes at the Equator and the Intertropical Convergence Zone. Geochem. Cosmochim. Acta 57, 4141–4163.
Murphy, A.E., Sageman, B.B., Hollander, D.J., Lyons, T.W., Brett, C.E., 2000. Black shale deposition and faunal overturn in the Devonian Appalachian basin: clastic starvation, seasonal water-column mixing, and efficient biolimiting nutrient recycling. Paleoceanography 15, 280–291.
Nesbitt, H.W., Young, G.M., 1989. Formation and diagenesis of weathering profiles. J. Geol. 97, 129–147.
Parrish, J.T., 1995. Paleogeography of Corg-rich rocks and the preservation versus production controversy. In: Huc, A.Y. (Ed.), Paleogeography, Paleoclimate, and Source Rocks, vol. 40. AAPG, Studies in Geology, pp. 1–20.

Pedersen, T.F., Calvert, S.E., 1990. Anoxia vs. productivity: what controls the formation of organic-carbon-rich sediments and sedimentary Rocks? AAPG Bull. 74, 454–466.
Peters, K.E., Walters, C.C., Moldowan, J.M., 2005. The Biomarker Guide. Cambridge University Press, Cambridge, UK.
Pi, D., Liu, C., Shields-Zhou, G.A., Jiang, S., 2013. Trace and rare earth element geochemistry of black shale and kerogen in the early Cambrian Niutitang Formation in Guizhou province, South China: constraints for redox environments and origin of metal enrichments. Precambrian Res. 225, 218–229.
Piper, D.Z., Perkins, R.B., 2004. A modern vs. Permian black shale—the hydrography, primary productivity, and water-column chemistry of deposition. Chem. Geol. 206, 177–197.
Qiu, X., Liu, C., Mao, G., Deng, Y., Wang, F., Wang, J., 2014. Late Triassic tuff intervals in the Ordos basin, Central China: their depositional, petrographic, geochemical characteristics and regional implications. J. Asian Earth Sci. 80, 148–160.
Qiu, X., Liu, C., Mao, G., Deng, Y., Wang, F., Wang, J., 2015. Major, trace and platinumgroup element geochemistry of the Upper Triassic nonmarine hot shales in the Ordos Basin, Central China. Appl. Geochem. 53, 42–52.
Remírez, M.N., Algeo, T.J., 2020. Paleosalinity determination in ancient epicontinental seas: a case study of the T-OAE in the Cleveland Basin (UK). Earth Sci. Rev. 201, 103072.
Rimmer, S.M., 2004. Geochemical paleoredox indicators in Devonian-Mississippian black shales, central Appalachian Basin (USA). Chem. Geol. 206, 373–391.
Roy, D.K., Roser, B.P., 2013. Climatic control on the composition of Carboniferous-Permian Gondwana sediments, Khalaspir basin, Bangladesh. Gondwana Res. 23, 1163–1171.
Schoepfer, S.D., Shen, J., Wei, H., Tyson, R.V., Ingall, E., Algeo, T.J., 2015. Total organic carbon, organic phosphorus, and biogenic barium fluxes as proxies for paleomarine productivity. Earth Sci. Rev. 149, 23–52.
Shen, J., Schoepfer, S.D., Feng, Q., Zhou, L., Yu, J., Song, H., Wei, H., Algeo, T.J., 2015. Marine productivity changes during the end-Permian crisis and Early Triassic recovery. Earth Sci. Rev. 149, 136–162.
Taylor, S.R., McLennan, S.M., 1985. The Continental Crust: its Composition and Evolution. Blackwell, Oxford, p. 312.
Thorpe, C., Lloyd, J.R., Law, GarethT.W., Burke, I.T., Shaw, S., Bryan, N.D., Morris, K., 2012. Strontium sorption and precipitation behaviour during bioreduction in nitrate impacted sediments. Chem. Geol. 306–307, 114–122.
Tribovillard, N., Algeo, T.J., Lyons, T., Riboulleau, A., 2006. Trace-metals as paleoredox and paleoproductivity proxies: an update. Chem. Geol. 232, 12–32.
Tribovillard, N., Algeo, T.J., Baudin, F., Riboulleau, A., 2012. Analysis of marine environmental conditions based on molybdenum–uranium covariation—applications to Mesozoic paleoceanography. Chem. Geol. 324, 46–58.
Tyson, R.V., 2001. Sedimentation rate, dilution, preservation and total organic carbon: some results of a modelling study. Org. Geochem. 32, 333–339.
Tyson, R.V., 2005. The “productivity versus preservation” controversy: cause, flaws, and resolution. Spec. Publ. 82, 17–33.
Vanos, B., Middelburg, J.J., Delange, G.J., 1991. Possible diagenetic mobilization of barium in sapropelic sediment from the eastern Mediterranean. Mar. Geol. 100 (1–4), 125–136.
Wang, A., Wang, Z., Liu, J., Xu, N., Li, H., 2021. The Sr/Ba ratio response to salinity in clastic sediments of the Yangtze River Delta. Chem. Geol. 559, 119923.
Wang, C., Wang, Q., Chen, G., He, L., Xu, Y., Chen, L., Chen, D., 2017. Petrographic and geochemical characteristics of the lacustrine black shales from the Upper Triassic Yanchang Formation of the Ordos Basin, China: implications for the organic matter accumulation. Mar. Petrol. Geol. 86, 52–65.
Wei, W., Algeo, T.J., 2020. Elemental proxies for paleosalinity analysis of ancient shales and mudrocks. Geochem. Cosmochim. Acta 287, 341–366.
Wille, M., NaGler, T.F., Lehmann, B., Schroder, S., Kramers, J.D., 2008. Hydrogen sulphide release to surface waters at the Precambrian/Cambrian boundary. Nature 453, 767–769.
Yang, Y., Li, W., Ma, L., 2005. Tectonic and stratigraphic controls of hydrocarbon systems in the Ordos basin: a multicycle cratonic basin in central China. AAPG Bull. 89 (2), 255–269.
Zhang, K., Liu, R., Liu, Z., Li, B., Han, J., Zhao, K., 2020. Influence of volcanic and hydrothermal activity on organic matter enrichment in the Upper Triassic Yanchang Formation, southern Ordos Basin, Central China. Mar. Petrol. Geol. 112, 104059.